

# Electronic band structure screening for Dirac points in Heuslers

Meza-Morales, Paul J.<sup>a</sup>, Fumarola, Alessandro<sup>a</sup>, Taliaironak, Volha<sup>a</sup>, Shirsekar, Afrid<sup>a</sup>, Kidner, Jonathan<sup>a</sup>, Ali, Zaheer<sup>a</sup>, Ali, Mazhar<sup>a,\*</sup>

<sup>a</sup>*Material Mind, Fremont, CA 94555, United States*

---

## Abstract

The Heusler compounds have provided a playground of material candidates for various technological applications based on their highly diverse and tunable properties, controlled by chemical composition and crystal structure. However, physical exploration of the Heusler chemical space *en masse* is impossible in practice, hindering the exploration of the chemical composition vs. properties relationship. Many of these applications are related to the Heuslers electron transport characteristics, which are embedded in their electronic band structure (EBS). Here we created a Heuslers dataset using the Materials Project (MP) database — retrieving both chemical composition and their EBSs. We then used machine learning to develop a model correlating the composition vs. number of Dirac points in the EBS for Heuslers and also other Cubic compounds by identifying said Dirac points using an automated algorithm as well as generating chemical composition and global crystal structure features. Our ML model captures the overall trend, as well as identifies significant electronic and global crystal structure features, however, the ML model suffered from significant variance due to the lack of site specific features. Future work on a methodology for handling atomic site specific features will allow ML models to better match the underlying quantum mechanics governing the properties (also based on site specific properties) and capture the electronic properties in a more generalized approach.

**Keywords:** Heusler, Dirac Points, Electronic Band Structure, Computational Material Science, Machine Learning

---

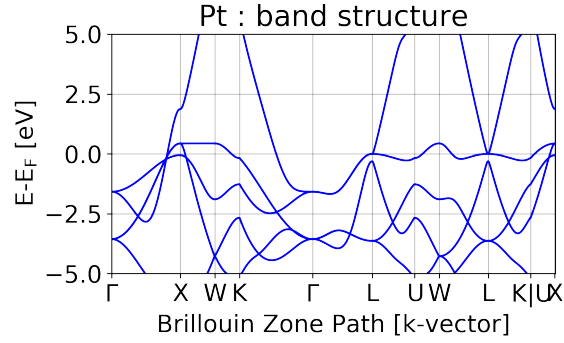
## 1. Introduction

Quantum materials (QMs)—materials in which quantum effects manifest non-classical properties—are expected to drive a variety of next generation technologies ranging from quantum computing[1, 2, 3] and sensing[4, 5, 6] to novel

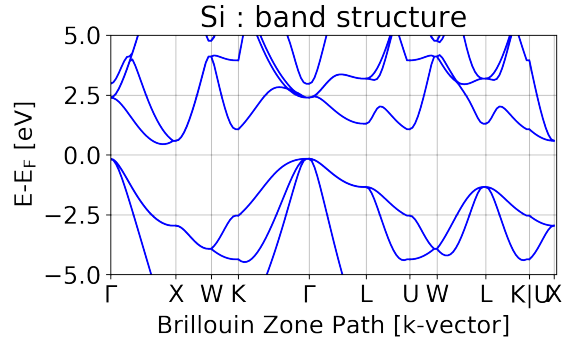
---

\*Corresponding author

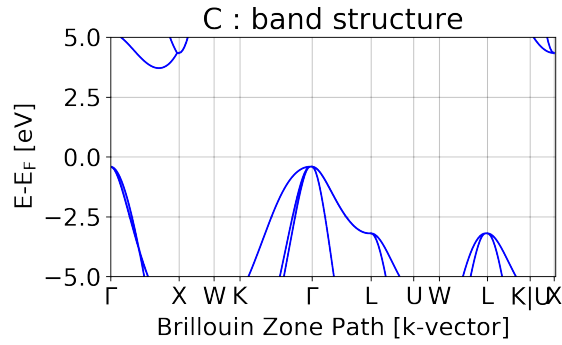
energy storage,[7, 8, 9, 3] telecommunication[10, 11, 12, 13, 14] and renewable energy generation solutions[15, 16, 17]. The electronic properties of these QMs are derived from their electronic band structures (EBSs); the spectrum of electronic energy states vs electron momenta, arising from the solutions of Schrodinger's equation for electrons in a periodic potential (i.e. crystal lattice, a periodic arrangement of atoms in space). For example, a classical material property, like metallic vs semiconducting vs insulating behavior, (see Figure 1) can be quickly understood by observing the energetic "band gaps" in the EBS. However in QMs, various non-classical properties can be gleaned from deeper patterns in the EBS such as "flat bands", "Dirac point", "Weyl points", "Nodal Lines", or spin-orbit coupled gap openings. For example, "flat bands" (Figure 2) are known to be associated with strong electron correlation and can contribute to properties like superconductivity, charge density wave ordering, magnetism, and more[18, 19, 20]. On the other hand, highly dispersive linear bands intersecting at a crossing point (a.k.a. Dirac point, Figure 2), are known to be associated with high carrier mobility, large Hall effects, spatially localized conduction and more[21, 22, 23, 24]. Combinations of Dirac points, Weyl points, Nodal Lines, flat band, spin-orbit coupled gap openings, and other patterns give rise to higher order electronic properties that are relevant to next generation materials and technologies. Hence predicting, identifying and understanding the patterns in the EBS is of great interest to the condensed matter, device physics and communities.



(a)



(b)



(c)

**Figure 1.** comparison of EBSs for metallic vs semiconducting vs insulating behavior using: a) metallic (Pt), b) semiconducting (Si), and c) insulating (Diamond). The energies of the band gaps are 4.34 eV for Diamond, 0.85 eV for Si and 0.0 eV for Pt. These EBSs were taken from Materials Project (MP) database [25, 26, 27] their MP-id are included in the legend of each material. [colors online]

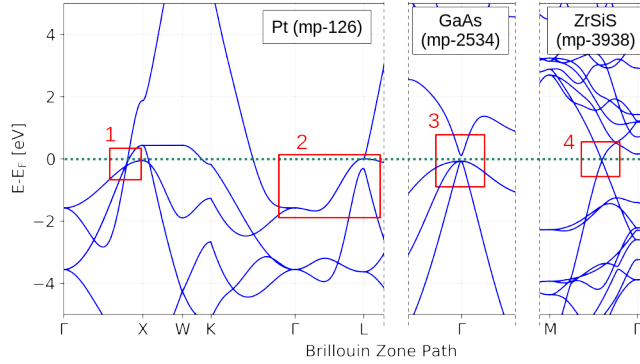


**Figure 2.** Deeper patterns in the EBS for Platinum (Pt), Gallium arsenide (GaAs), and Zirconium Silicon Sulfide (ZrSiS). Red boxes correspond to 1. tilted Dirac point, 2. Nodal line, 3. local flat band with other highly dispersive bands, and 4. Dirac point at the Fermi level. The EBSs were taken from Materials Project (MP) database,[25] their MP-id are included in the legend of each material. [colors online]

Currently, electronic band structures are calculated using Density Functional Theory (DFT), a powerful method for quantum mechanical calculations of many body systems. While successful at generating accurate results for nonmagnetic and low spin-orbit coupled systems, DFT calculations become computationally expensive as non-idealities of the model are considered. This includes crystals defects, magnetism, strong spin-orbit coupling (SOC), large unit cells, strong electron correlation ( $J$ ), etc. It is also time consuming to carry out these calculations en-masse; while the Materials Project[28] has approximately 100K materials in the database, this is a small number compared to the more than  $10^{18}$  possible material combinations predicted to exist, and carrying out full DFT + SOC + U + magnetism calculations on that dataset is simply unrealistic. While supercomputers and new exchange-correlation functional development aid in expanding the reach of DFT, another compelling approach may be to use artificial intelligence (AI) algorithms—such as machine learning (ML)—to predict patterns in EBSs from a chemical composition and crystal structure without carrying out intensive DFT calculations. Thus, by training on known DFT computed EBSs and learning what chemical compositions/structural features drive certain electronic structure patterns, it is possible to use AI models as a rapid screening tool and identify promising material classes or candidates for deeper theoretical and experimental investigation as well as to discover new materials with desired properties. These machine learning methods center around the core idea of learning against the hidden correlations of the material’s structures with the physical property of relevance for a subgroup of materials, where the property values are either computationally computed or experimentally available, to quantitatively establish a structure-property relationship. The insight gained from the subgroup of materials is then utilized to deliver predictions on the property for all materials in the parent group, thus eliminating the need for spending time consuming computational or experimental resources for these

structures.[29, 30, 31, 32, 33] In the case where there is a paucity of experimental physical property data but a particular pattern in the electronic band structure is known to relate to a physical property of interest, the correlation methodology can become focused on learning against the correlations of the material’s structure with the electronic band structure. This approach has precedence, being used in prediction of novel thermoelectrics,[34, 35, 36] construction materials,[37] solar cell materials,[38, 39] and more.

To begin this approach for QMs, first we narrow our materials of interest to a particularly successful class of QM materials, the Heusler family,[40, 41, 42, 43, 44, 45] which has attracted major interest from the community for their wide-ranging applications in the domain of spintronics,[10, 12, 42] thermoelectrics,[17, 44, 45] superconductors,[20, 46, 47, 48] solar-cells,[49, 50, 51, 52] multifunctional topological insulators,[53, 54, 55] etc. Chemically, they are ternary compounds which can be further distinguished into “half” and “full” Heuslers based on their stoichiometry. The chemical formula for half-Heuslers and full-Heuslers are of the form XYZ (1:1:1) and  $X_2YZ$  (2:1:1) respectively, where X and Y generally have a cationic character (*d*-block elements—transition metals) and Z is expected to be the anionic counterpart (*p*-block elements). Crystallographically, Heusler compounds exhibit a face-centered cubic crystal structure, as depicted on Figure 3, with space groups 216 and 225 for half-Heuslers and full-Heuslers respectively. As a myriad of chemical choices are possible with the X, Y and Z sites, Heusler’s material properties can be tuned by altering the composition, which can be leveraged for accelerating material development in applications.

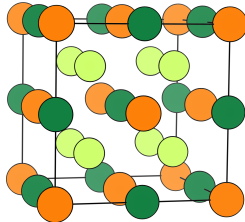


**Figure 3.** Illustrative full-Heusler crystal— $MnCu_2Al$ . Al, Mn, and Cu are colored in orange, green, and lime respectively. Structure taken from Materials Project[25] (MP-id: mp-3574). [colors online]

The chemical composition to EBS dependency for Heuslers is, however, a complicated relationship, being dependent on which atoms are located at which atomic site in the crystal structure and the resulting interaction of their atomic orbitals.[56, 57, 58] A challenge in Heusler design is to predict how the chemical composition and crystallographic arrangement influences EBSs without requiring exhaustive DFT calculation. However, given the large number of possibilities, comprising  $> 1500$  known members with an exponentially larger number of possibilities if different atomic crystal arrangements are considered for a given composition, first-principles calculation and learning of their influence on the EBS is unmanageable, making it a good test bed for attempting to use AI and

ML as mentioned above.

We create a Heuslers dataset using the Materials Project (MP) database;<sup>[25]</sup> considering compounds with cubic crystal structures and general formulas XYZ and  $X_2YZ$ , which correspond to space groups 216 and 225 (a total 276 compounds). The EBSs are also retrieved from the MP which are computed using DFT calculations. Using this Heuslers dataset along with the python library Matminer<sup>[59, 60]</sup> for rapid features extraction, we developed an ML model that correlates Heusler’s chemical compositions with their EBSs; specifically with the number of band crossings within a specific range of the ground state energy ( $\pm 1$  eV). We extract the number of crossings from the EBS using an automated algorithm to mine the EBS for that particular pattern. The ML model is then developed using the XGBoost algorithm<sup>[61, 62]</sup>—a parallel tree boosting technique under Gradient Boosting framework—to train the model as a function of periodic table properties of the materials constituent elements (chemical composition) and global crystal structure parameters. Also, since the Heuslers dataset consists of a relatively small number of compounds (276), we also created a dataset of cubic compounds removing the restriction of specific transition metal atoms for X and Y elements, and  $p$ -block atoms for Z elements, but retaining the space groups 216 and 225. This “Cubic dataset” consists of 3751 structures, and is used to benchmark the ML models and understand the generalizability of the insight gained from the Heuslers dataset.

## 2. Methodology

### 2.1. Materials Data-set

The data used in this work is entirely sourced from the the Materials Project with  $\sim 76\,240$  entries of EBSs calculated via DFT. For the Heusler and Cubic dataset with space groups of 216 and 225, the whole MP database was searched—using the pymatgen python library<sup>[63]</sup>—for materials with cubic crystal symmetry (space groups 216 and 225) which were then downloaded including their chemical, structural, EBS. The total number of materials found after this search was 276 and 3751 for the Heuslers and Cubic datasets respectively; and are available at GitHub Link. Heuslers dataset is formed by 107 and 169 half (space group 216) and full (space group 225) Heuslers respectively. Consisting of compounds comprised by X and Y elements from groups 1 to 12 ( $s$  and  $d$  blocks) and periods 4 to 6; and Z elements from groups 13 to 16 and ( $p$ -block) periods 3 to 6 (see Figure 4(a)). On the other hand, the Cubic dataset consist of compounds comprised by X and Y elements from groups 1 to 12 ( $s$  and  $d$  blocks) and periods 1 to 6; and Z elements from groups 13 to 17 ( $p$ -block) and periods 2 to 6 (see Figure 4(b)). The Heuslers dataset compounds are constrained to have for X and Y elements  $s$  and  $d$  blocks atoms whereas for Z element  $p$ -block atoms. These constraints are removed for the Cubic dataset compounds i.e. X, Y, and Z can be either  $s$ ,  $d$  or  $p$ -block elements. However, the symmetry constraints (space groups 216 or 225) were retained. Noteworthy, X, Y and Z elements in the Cubic dataset exhibit counting ranging from  $\sim 75$  to

225, highlighting fluorine (F) with an outlier counting of 450. In contrast, X, Y and Z elements in the Heuslers dataset exhibit counting ranging from  $\sim 7$  to 55.

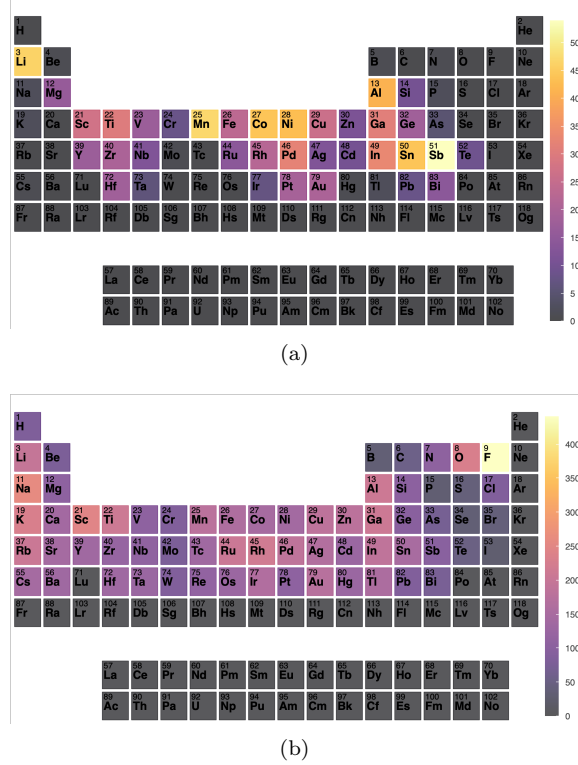


**Figure 4.** a) Periodic table heatmap for element appearance on Heuslers dataset, b) Periodic table heatmap for element appearance on the Cubic dataset. Elements are colored according to their appearance on in the respective datasets, gray corresponds to no appearance and yellow for maximum appearance. [Colors online]

## 2.2. Electronic Band Structure: Dirac points identification - Number of Crossings

EBSs are imported as a  $N \cdot K$  matrix of energy value, with  $N$  being the number of bands calculated by the DFT calculation and  $K$  being the number of momentum-points sampled along the MP-recommended BZ path. The MP database uses the BZ path convention presented in [64]. Specifically we identify Dirac points over the EBSs—termed ‘number of crossings’—within a specific range of the ground state energy ( $\pm 1$  eV). The number of crossings distributions for the Heusler and Cubic datasets are shown in Figure 5. In both cases, the distributions are right skewed but despite the Cubic dataset having 14 times more compounds than Heuslers dataset, both number of crossings distributions have close medians  $\sim 8$ . Suggesting the distributions shape correspond to the number of crossings natural variation instead of an data errors or sampling

problems. Also, more than 50% of the Heuslers number of crossings range consists of outlier data points (see box plot on Figure 5(a)), whereas the Cubic dataset distribution has almost no outliers (see box plot on Figure 5(b)).

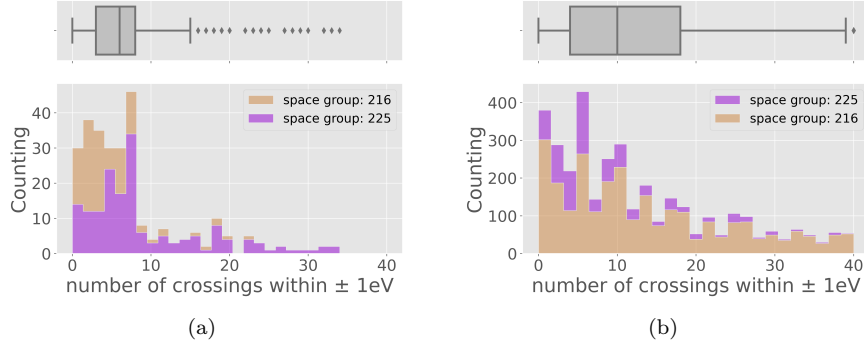


**Figure 5.** Distribution of number of crossings on the EBS (within  $\pm 1$  eV) a) Heuslers dataset, and b) Cubic dataset. [Colors online]

### 2.3. Machine Learning Modeling

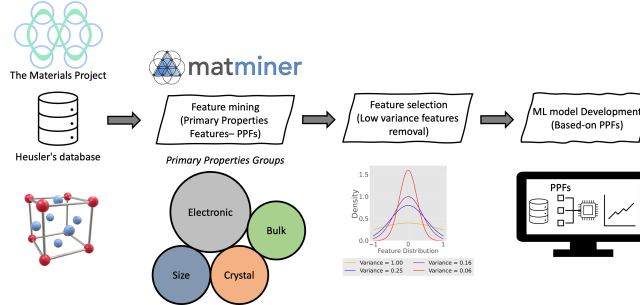


**Figure 6.** ML modeling flowchart; which consist of: 1) data minig and data sets creation, 2) features extraction, 3) features selection, and 4) ML models development. [Colors online]

A Machine learning (ML) pipeline is implemented to develop models that can predict the number of crossings in the EBSs (within  $\pm 1$  eV) for the Heuslers and Cubic datasets. From the logic that the EBS's number of crossings depends on the nature of the atoms within the crystal lattice and their arrangement with each other, the models take as the input as the identities of the atoms in the crystal—encoded as elemental properties—producing, as output, estimates of the number of crossings (within  $\pm 1$  eV). A general flowchart for ML pipeline is presented on Figure 6; specifically, the features engineering consists of two main steps: 1) Feature extraction, and 2) Feature selection. For features extraction, atom properties are taken from the python library Matminer[28, 60] for both datasets and named primary properties features (PPFs) and are classified into 4

groups: bulk, electronic, size, and crystal. Matminer creates overall features i.e., for a specify elemental composition of a crystal, and identifies the minimum and maximum values for a given property. We consider a total of 53 PPFs including e.g, electronegativity, covalent radius, volume per atom, etc. The PPFs, for developing the ML models, are selected based on the low-variance criterion; i.e. any given PPF which consists of a constant value in the 80 % or more of its values distribution, or whose variance is  $\leq 0.16$ , are removed. See SI for the full list of PPFs and their values.

The ML regression models and features importance are performed with the XGBoost approach [62, 61]. XGBoost provides a parallel tree boosting algorithm [65] that contains three elements: 1) a minimizing loss function, 2) a weak learner (regression tree) for making predictions, and 3) an additive model that combines weak learners into strong ones in order to minimize the loss function. In our model, the loss function is the root mean square error (rmse) between the computed and the ML predicted band structure number of crossings (within  $\pm 1$  eV). The regression trees weak learners are set by specifying the learning rate, gamma, max\_depth, max\_delta\_step, subsample, colsample\_bytree, colsample\_bylevel, lambda, alpha, gamma, min\_child\_weight, and scale\_pos\_weight parameters. Bayesian optimization and cross validation (shuffle-split (7-folded)) algorithms, as implemented in scikit-optimize python library,[66] are employed to identify the best combinations of hyperparameter values (e.g., max depth, number of threads, etc.) during the ML-models development. The Feature importance score (using gain scoring) is estimated to identify those PPFs that most influence the prediction of band structure number of crossings (within  $\pm 1$  eV). 70 % of the dataset is assigned to the training set, whereas the remaining 30 % is assigned to the testing set. The training and test sets are assessed based on the mean absolute errors (MAEs) between the calculated (with DFT) and the predicted (with ML) as illustrated in eq. 1:

$$\text{MAE} = \frac{\sum_i^N |n_i^{\text{DFT}} - n_i^{\text{ML}}|}{N} \quad (1)$$

where  $n$  stands for band structure number of crossing (within  $\pm 1$  eV).

### 3. Results

#### 3.1. Machine Learning Model

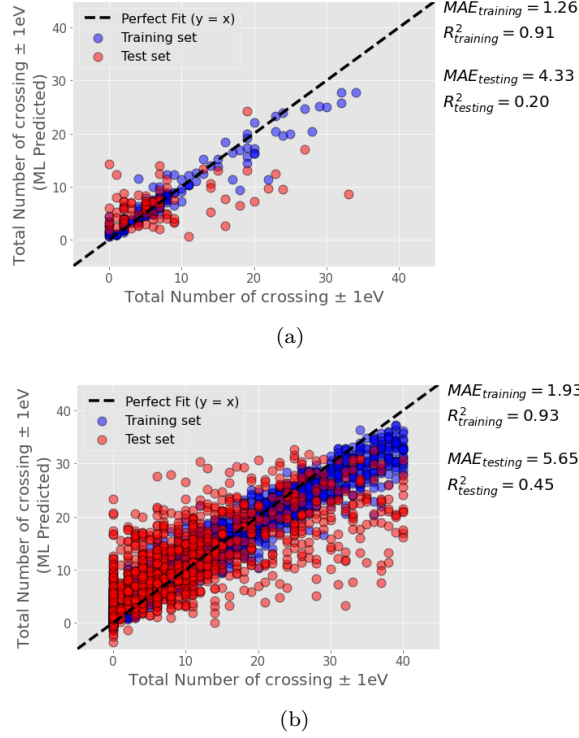
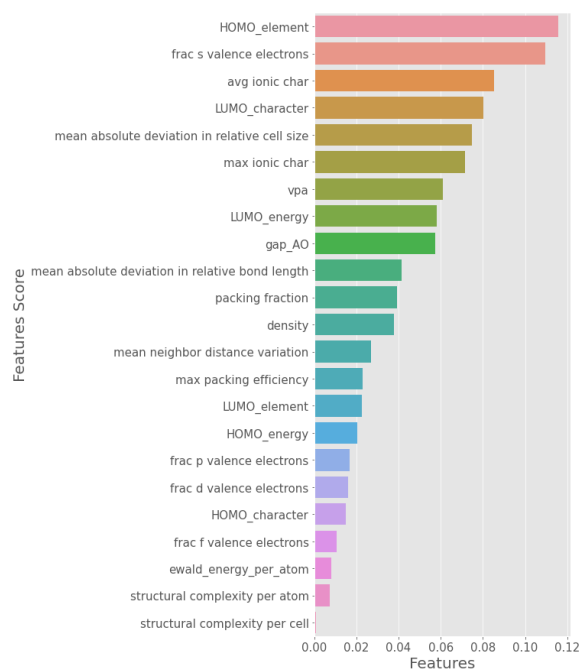


**Figure 7.** ML model parity plot comparing DFT-calculated with ML predicted values for band structure number of crossing (within  $\pm 1$  eV) a) Heuslers dataset, and b) Cubic dataset. [Colors online]

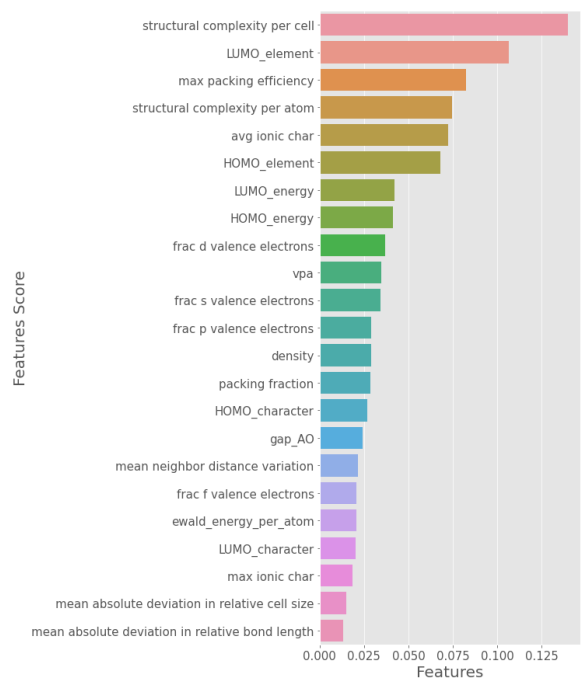
Figures 7(a) and 7(b) compare, in parity plots, the ML predictions with DFT-calculated EBS's number of crossings (within  $\pm 1$  eV) for the Heuslers and Cubic datasets respectively. For these models, the coefficient of determination ( $R^2$ ) of training and testing sets are 0.91 and 0.20, and 0.93 and 0.45 for the Heuslers and Cubic datasets respectively. Similarly, the mean absolute errors (MAEs) are 1.26 and 4.43, and 1.93 and 5.65. Comparing the training and testing set's MAEs with the respective number of crossings distribution, the MAEs correspond to the 6.74 % and 28.9 %, and 9.50 % and 20.1 % of distribution values, for the Heuslers and Cubic datasets respectively. First, the ( $R^2$ ) of the testing set for the Cubic dataset has improved by nearly a factor of two from the Heusler dataset, despite the training statistics being nearly the same. This implies that the Heusler dataset size, which was only about 1/14 the size of the cubic dataset, was a limiting factor. However the MAE of the Cubic dataset's test set is very similar to the MAE of the Heusler dataset's test set suggesting

that the ML performance observed for the Heuslers compounds is not only consequence of the dataset size. And while the Cubic dataset predictions do show a clear linear tendency, the accuracy of the predictions leave much to be desired. Since the ML models features lack of crystal site specific information—which can better encode chemical composition, atoms arrangement, and chemical environment effects, as DFT calculations do—their prediction performance is affected impacting the ML models variance.

Regarding the ML models features importance, Figure 8 shows the bar plots for the features important score (gain). Highlighting for both ML models—among the first 10 most important features—the “HOMO element”, “avg. ionic char”, “vpa” (volume per atom), and “LUMO energy”. All of these features are associated with both electronic and crystal primary properties. Moreover, by grouping features importance scores—based on the electronic and crystal categories—the electronic properties have an slightly higher importance in predicting the number of crossing on the ML models, as expected from comparison to DFT. Among the electronic features, the ones related to HOMO and LUMO frontier levels appear in both models; similarly, for crystal features, the “structural complexity per cell”, a composite feature related to the local coordination of the atoms, is ranked highly, again as expected from DFT. In the case of bulk properties like density, they do not have a significant importance among the ML models features, as expected from DFT. Taken together, these results imply the model did begin to capture the correct underlying physics driving the target result, but was hampered by the lack of site-specific features. Among the global features it had access to, it ranked most highly the ones which were at least partially site-specific; structural complexity, atomic orbitals, etc.



(a)



(b)

**Figure 8.** a) Feature important scoring (Gain) for a) Heuslers compounds ML model, and b) Cubic compounds ML model. [Colors online]

## 4. Conclusions

In this work, we used machine learning to develop a model correlating composition vs. number of Dirac points (called the number of crossings) in the electronic band structures for Heuslers and other Cubic compounds by identifying said crossings using an automated algorithm as well as generating chemical composition and global crystal structure features. In general, our ML model captured the overall trend in the Heuslers, predicting the EBS number of crossings; however, the ML model (parity plot) suffered from significant variance. The Heuslers datasets size (276 compounds) was not the limiting factor in regards of the variance; an additional ML model was created for the larger dataset of Cubic compounds of size ( $\sim 3800$  compounds), and it also exhibited a similar variance. This is, however, within expectation, due to the nature of the EBS where it is well understood that atomic site specific properties determine the band structure. A methodology for handling atomic site specific features has to be developed such that ML models can incorporate their description, in a better match to the underlying quantum mechanics governing the properties, and capture the electronic properties in a more generalized approach. This atomic site specific approach is, however, difficult due to the feature dimensionality dramatically increasing as, for example, the number of possible atomic sites (up to 64) convolved with the number of possible elements at each site (up to 118) convolved with the number of atomic orbitals at each site (up to 14), becomes unuseably large. Thus, an open challenge for future applications of ML in electronic materials intelligence, requires the development of featurizers that are able to generate atomic site features but also encoding them into artificial structural features to reduce the dimensionality.

## References

- [1] L. Bassman, M. Urbanek, M. Metcalf, J. Carter, A. F. Kemper, W. A. de Jong, Simulating quantum materials with digital quantum computers, *Quantum Science and Technology* 6 (4) (2021) 043002.
- [2] W. Han, Y. Otani, S. Maekawa, Quantum materials for spin and charge conversion, *npj Quantum Materials* 3 (1) (2018) 1–16.
- [3] C. N. Lau, F. Xia, L. Cao, Emergent quantum materials, *MRS Bulletin* 45 (5) (2020) 340–347.
- [4] L. Zhu, Z. L. Wang, Progress in piezotronics and piezo-phototronics of quantum materials, *Journal of Physics D: Applied Physics* 52 (34) (2019) 343001.
- [5] Z. Hennighausen, S. Kar, Twistronics: A turning point in 2d quantum materials, *Electronic Structure* 3 (1) (2021) 014004.

- [6] S. E. Crawford, R. A. Shugayev, H. P. Paudel, P. Lu, M. Syamlal, P. R. Ohodnicki, B. Chorpene, R. Gentry, Y. Duan, Quantum sensing for energy applications: Review and perspective, *Advanced Quantum Technologies* 4 (8) (2021) 2100049.
- [7] C. Broholm, I. Fisher, J. Moore, M. Murnane, A. Moreo, J. Tranquada, D. Basov, J. Freericks, M. Aronson, A. MacDonald, et al., Basic research needs workshop on quantum materials for energy relevant technology, Tech. rep., USDOE Office of Science (SC)(United States) (2016).
- [8] Y. Tokura, M. Kawasaki, N. Nagaosa, Emergent functions of quantum materials, *Nature Physics* 13 (11) (2017) 1056–1068.
- [9] B.-R. Koo, H.-J. Ahn, Research impact on emerging quantum materials for electrochromic applications, *Israel Journal of Chemistry* 59 (8) (2019) 673–678.
- [10] A. Birsan, V. Kuncser, Zr-based heusler compounds for biomedical spintronic applications, in: *Magnetic Materials and Magnetic Levitation*, IntechOpen, 2020, p. 89.
- [11] J. Wei, X. Chu, X.-Y. Sun, K. Xu, H.-X. Deng, J. Chen, Z. Wei, M. Lei, Machine learning in materials science, *InfoMat* 1 (3) (2019) 338–358.
- [12] S. A. Khandy, I. Islam, D. C. Gupta, A. Laref, Full heusler alloys (co<sub>2</sub>tasi and co<sub>2</sub>tage) as potential spintronic materials with tunable band profiles, *Journal of Solid State Chemistry* 270 (2019) 173–179.
- [13] G. Grigaliūnaitė-Vonševičienė, B. Vengalis, A. Maneikis, R. Juškėnas, Magnetic and electrical properties of postannealed co<sub>2</sub>mnsi heusler alloy films, *Applied Nanoscience* 10 (7) (2020) 2229–2237.
- [14] C. Fowley, K. Rode, Y.-C. Lau, N. Thiyagarajah, D. Betto, K. Borisov, G. Atcheson, E. Kampert, Z. Wang, Y. Yuan, et al., Magnetocrystalline anisotropy and exchange probed by high-field anomalous hall effect in fully compensated half-metallic mn<sub>2</sub>ru<sub>x</sub>ga thin films, *Physical Review B* 98 (22) (2018) 220406.
- [15] P. K. Kamlesh, R. Agarwal, U. Rani, A. S. Verma, First-principles calculations of inherent properties of rb based state-of-the-art half-heusler compounds: promising materials for renewable energy applications, *Physica Scripta* 96 (11) (2021) 115802.
- [16] P. K. Kamlesh, R. Agrawal, U. Rani, A. S. Verma, Comprehensive ab-initio calculations of al<sub>x</sub> (x= p, as and sb) half-heusler compounds: Stabilities and applications as green energy resources, *Materials Chemistry and Physics* 275 (2022) 125233.

- [17] S. H. Zaferani, R. Ghomashchi, D. Vashaee, Strategies for engineering phonon transport in heusler thermoelectric compounds, *Renewable and Sustainable Energy Reviews* 112 (2019) 158–169.
- [18] L. Balents, C. R. Dean, D. K. Efetov, A. F. Young, Superconductivity and strong correlations in moiré flat bands, *Nature Physics* 16 (7) (2020) 725–733.
- [19] Z. S. Yang, A. M. Ferrenti, R. J. Cava, Testing whether flat bands in the calculated electronic density of states are good predictors of superconducting materials, *Journal of Physics and Chemistry of Solids* 151 (2021) 109912.
- [20] Y. Hu, S. M. Teicher, B. R. Ortiz, Y. Luo, S. Peng, L. Huai, J. Ma, N. Plumb, S. D. Wilson, J.-F. He, et al., Charge-order-assisted topological surface states and flat bands in the kagome superconductor  $\text{CsV}_3\text{Sb}_5$ , arXiv preprint arXiv:2104.12725.
- [21] J. Falson, M. Kawasaki, A review of the quantum hall effects in  $\text{MgZnO}/\text{ZnO}$  heterostructures, *Reports on Progress in Physics* 81 (5) (2018) 056501.
- [22] C. Zhang, Y. Zhang, H.-Z. Lu, X. Xie, F. Xiu, Cycling fermi arc electrons with weyl orbits, *Nature Reviews Physics* 3 (9) (2021) 660–670.
- [23] M. M. H. Polash, S. Yalameha, H. Zhou, K. Ahadi, Z. Nourbakhsh, D. Vashaee, Topological quantum matter to topological phase conversion: Fundamentals, materials, physical systems for phase conversions, and device applications, *Materials Science and Engineering: R: Reports* 145 (2021) 100620.
- [24] T. Liang, Q. Gibson, M. N. Ali, M. Liu, R. J. Cava, N. P. Ong, Ultrahigh mobility and giant magnetoresistance in the dirac semimetal  $\text{Cd}_3\text{As}_2$ , *Nature Materials* 14 (3) (2015) 280–284. doi:10.1038/nmat4143. URL <https://doi.org/10.1038/nmat4143>
- [25] A. Jain, S. P. Ong, G. Hautier, W. Chen, W. D. Richards, S. Dacek, S. Cholia, D. Gunter, D. Skinner, G. Ceder, K. a. Persson, The Materials Project: A materials genome approach to accelerating materials innovation, *APL Materials* 1 (1) (2013) 011002. doi:10.1063/1.4812323. URL <http://link.aip.org/link/AMPADS/v1/i1/p011002/s1&Agg=doi>
- [26] A. Jain, S. P. Ong, G. Hautier, W. Chen, W. D. Richards, S. Dacek, S. Cholia, D. Gunter, D. Skinner, G. Ceder, et al., Commentary: The materials project: A materials genome approach to accelerating materials innovation, *APL materials* 1 (1) (2013) 011002.
- [27] S. P. Ong, S. Cholia, A. Jain, M. Brafman, D. Gunter, G. Ceder, K. A. Persson, The materials application programming interface (api): A simple, flexible and efficient api for materials data based on representational state transfer (rest) principles, *Computational Materials Science* 97 (2015) 209–215.

- [28] L. Ward, A. Dunn, A. Faghaninia, N. E. Zimmermann, S. Bajaj, Q. Wang, J. Montoya, J. Chen, K. Bystrom, M. Dylla, et al., Matminer: An open source toolkit for materials data mining, *Computational Materials Science* 152 (2018) 60–69.
- [29] P. Z. Moghadam, S. M. Rogge, A. Li, C.-M. Chow, J. Wieme, N. Moharrami, M. Aragoes-Anglada, G. Conduit, D. A. Gomez-Gualdron, V. Van Speybroeck, et al., Structure-mechanical stability relations of metal-organic frameworks via machine learning, *Matter* 1 (1) (2019) 219–234.
- [30] W. Sun, Y. Zheng, K. Yang, Q. Zhang, A. A. Shah, Z. Wu, Y. Sun, L. Feng, D. Chen, Z. Xiao, et al., Machine learning-assisted molecular design and efficiency prediction for high-performance organic photovoltaic materials, *Science advances* 5 (11) (2019) eaay4275.
- [31] T. Zhou, Z. Song, K. Sundmacher, Big data creates new opportunities for materials research: a review on methods and applications of machine learning for materials design, *Engineering* 5 (6) (2019) 1017–1026.
- [32] B. R. Goldsmith, J. Esterhuizen, J.-X. Liu, C. J. Bartel, C. Sutton, Machine learning for heterogeneous catalyst design and discovery.
- [33] T. Toyao, Z. Maeno, S. Takakusagi, T. Kamachi, I. Takigawa, K.-i. Shimizu, Machine learning for catalysis informatics: recent applications and prospects, *Acs Catalysis* 10 (3) (2019) 2260–2297.
- [34] X. Jia, Y. Deng, X. Bao, H. Yao, S. Li, Z. Li, C. Chen, X. Wang, J. Mao, F. Cao, J. Sui, J. Wu, C. Wang, Q. Zhang, X. Liu, Unsupervised machine learning for discovery of promising half-heusler thermoelectric materials, *npj Computational Materials* 8 (1) (2022) 34. doi:10.1038/s41524-022-00723-9.  
URL <https://doi.org/10.1038/s41524-022-00723-9>
- [35] G. S. Na, S. Jang, H. Chang, Predicting thermoelectric properties from chemical formula with explicitly identifying dopant effects, *npj Computational Materials* 7 (1) (2021) 106. doi:10.1038/s41524-021-00564-y.  
URL <https://doi.org/10.1038/s41524-021-00564-y>
- [36] Y. Sheng, Y. Wu, J. Yang, W. Lu, P. Villars, W. Zhang, Active learning for the power factor prediction in diamond-like thermoelectric materials, *npj Computational Materials* 6 (1) (2020) 171. doi:10.1038/s41524-020-00439-8.  
URL <https://doi.org/10.1038/s41524-020-00439-8>
- [37] U. Masood Chaudry, K. Hamad, T. Abuhmed, Machine learning-aided design of aluminum alloys with high performance, *Materials Today Communications* 26 (2021) 101897. doi:<https://doi.org/10.1016/j.mtcomm.2020.101897>.  
URL <https://www.sciencedirect.com/science/article/pii/S2352492820329081>

- [38] K. Choudhary, M. Bercx, J. Jiang, R. Pachter, D. Lamoen, F. Tavazza, Accelerated discovery of efficient solar cell materials using quantum and machine-learning methods, *Chemistry of Materials* 31 (15) (2019) 5900–5908. doi:10.1021/acs.chemmater.9b02166.  
URL <https://doi.org/10.1021/acs.chemmater.9b02166>
- [39] Y. Miyake, A. Saeki, Machine learning-assisted development of organic solar cell materials: Issues, analyses, and outlooks, *The Journal of Physical Chemistry Letters* 12 (51) (2021) 12391–12401, pMID: 34939806. arXiv:<https://doi.org/10.1021/acs.jpclett.1c03526>, doi:10.1021/acs.jpclett.1c03526.  
URL <https://doi.org/10.1021/acs.jpclett.1c03526>
- [40] I. Galanakis, Theory of heusler and full-heusler compounds, in: *Heusler Alloys*, Springer, 2016, pp. 3–36.
- [41] T. Graf, S. S. Parkin, C. Felser, Heusler compounds—a material class with exceptional properties, *IEEE Transactions on Magnetics* 47 (2) (2010) 367–373.
- [42] F. Casper, T. Graf, S. Chadov, B. Balke, C. Felser, Half-heusler compounds: novel materials for energy and spintronic applications, *Semiconductor Science and Technology* 27 (6) (2012) 063001.
- [43] T. Graf, C. Felser, S. S. Parkin, Simple rules for the understanding of heusler compounds, *Progress in solid state chemistry* 39 (1) (2011) 1–50.
- [44] S. J. Poon, Recent advances in thermoelectric performance of half-heusler compounds, *Metals* 8 (12) (2018) 989.
- [45] S. Chibani, O. Arbouche, M. Zemouli, Y. Benallou, K. Amara, N. Chami, M. Ameri, M. El Keurti, First-principles investigation of structural, mechanical, electronic, and thermoelectric properties of half-heusler compounds ruvx (x= as, p, and sb), *Computational Condensed Matter* 16 (2018) e00312.
- [46] H. Xiao, T. Hu, W. Liu, Y. Zhu, P. Li, G. Mu, J. Su, K. Li, Z. Mao, Superconductivity in the half-heusler compound tbpdbi, *Physical Review B* 97 (22) (2018) 224511.
- [47] H. Uzunok, E. Karaca, S. Bağcı, H. Tütüncü, Physical properties and superconductivity of heusler compound liga2rh: A first-principles calculation, *Solid State Communications* 311 (2020) 113859.
- [48] L. Kautzsch, F. Mende, G. H. Fecher, J. Winterlik, C. Felser, Are aupdtm (t= sc, y and m= al, ga, in), heusler compounds superconductors without inversion symmetry?, *Materials* 12 (16) (2019) 2580.

- [49] M. Abdel-Shakour, T. H. Chowdhury, K. Matsuishi, I. Bedja, Y. Moritomo, A. Islam, High-efficiency tin halide perovskite solar cells: The chemistry of tin (ii) compounds and their interaction with lewis base additives during perovskite film formation, *Solar rrl* 5 (1) (2021) 2000606.
- [50] G. Murtaza, T. Alshahrani, R. A. Khalil, Q. Mahmood, T. H. Flemban, H. Althib, A. Laref, Lead free double perovskites halides  $\text{x}_2\text{agtlcl}_6$  ( $\text{x} = \text{rb}, \text{cs}$ ) for solar cells and renewable energy applications, *Journal of Solid State Chemistry* 297 (2021) 121988.
- [51] B. Wang, L. Yang, C. Dall’Agnese, A. K. Jena, S.-i. Sasaki, T. Miyasaka, H. Tamiaki, X.-F. Wang, Photoactive zn-chlorophyll hole transporter-sensitized lead-free  $\text{cs}_2\text{agbibr}_6$  perovskite solar cells, *Solar RRL* 4 (7) (2020) 2000166.
- [52] M. Leoncini, A.-L. Capodilupo, D. Altamura, C. Giannini, G. Accorsi, E. Fabiano, A. Rizzo, G. Gigli, S. Gambino, Correlating the chemical structure and charge transport ability of dibenzofulvene-based hole transporting materials for stable perovskite solar cells, *Journal of Materials Chemistry C*.
- [53] R. M. Sattigeri, P. K. Jha, Dimensional engineering of a topological insulating phase in half-heusler ligas, *Scientific Reports* 11 (1) (2021) 1–10.
- [54] C. Barman, A. Alam, Topological phase transition in the ternary half-heusler alloy  $\text{zr}_2\text{rbi}$ , *Physical Review B* 97 (7) (2018) 075302.
- [55] Y. Zhang, X. Xu, Machine learning modeling of lattice constants for half-heusler alloys, *AIP Advances* 10 (4) (2020) 045121.
- [56] M. Ojala, G. C. Garriga, Permutation tests for studying classifier performance., *Journal of Machine Learning Research* 11 (6).
- [57] J. Ma, V. I. Hegde, K. Munira, Y. Xie, S. Keshavarz, D. T. Mildebrath, C. Wolverton, A. W. Ghosh, W. Butler, Computational investigation of half-heusler compounds for spintronics applications, *Physical Review B* 95 (2) (2017) 024411.
- [58] J. Ma, J. He, D. Mazumdar, K. Munira, S. Keshavarz, T. Lovorn, C. Wolverton, A. W. Ghosh, W. H. Butler, Computational investigation of inverse heusler compounds for spintronics applications, *Physical Review B* 98 (9) (2018) 094410.
- [59] L. Ward, A. Dunn, A. Faghaninia, N. E. Zimmermann, S. Bajaj, Q. Wang, J. Montoya, J. Chen, K. Bystrom, M. Dylla, K. Chard, M. Asta, K. A. Persson, G. J. Snyder, I. Foster, A. Jain, Matminer: An open source toolkit for materials data mining, *Computational Materials Science* 152 (2018) 60–69. doi:<https://doi.org/10.1016/j.commatsci.2018.05.018>.  
URL <https://www.sciencedirect.com/science/article/pii/S0927025618303252>

- [60] Matminer library, <https://hackingmaterials.lbl.gov/matminer>, accessed: 2022-01-30.
- [61] T. Chen, C. Guestrin, Xgboost: A scalable tree boosting system, in: Proceedings of the 22nd acm sigkdd international conference on knowledge discovery and data mining, ACM, 2016, pp. 785–794.
- [62] T. Chen, T. He, M. Benesty, V. Khotilovich, Y. Tang, Xgboost: extreme gradient boosting, R package version 0.4-2 (2015) 1–4.
- [63] S. P. Ong, W. D. Richards, A. Jain, G. Hautier, M. Kocher, S. Cholia, D. Gunter, V. L. Chevrier, K. A. Persson, G. Ceder, Python materials genomics (pymatgen): A robust, open-source python library for materials analysis, Computational Materials Science 68 (2013) 314–319. doi:<https://doi.org/10.1016/j.commatsci.2012.10.028>.  
URL <https://www.sciencedirect.com/science/article/pii/S0927025612006295>
- [64] W. Setyawan, S. Curtarolo, High-throughput electronic band structure calculations: Challenges and tools, Computational materials science 49 (2) (2010) 299–312.
- [65] K. Chen, R. Lu, C. Wong, G. Sun, L. Heck, B. Tseng, Trada: tree based ranking function adaptation, in: Proceedings of the 17th ACM conference on Information and knowledge management, ACM, 2008, pp. 1143–1152.
- [66] T. Head, M. Kumar, H. Nahrstaedt, G. Louppe, I. Shcherbatyi, scikit-optimize/scikit-optimize (Sep. 2020). doi:[10.5281/zenodo.4014775](https://doi.org/10.5281/zenodo.4014775).  
URL <https://doi.org/10.5281/zenodo.4014775>